JMEPEG
https://doi.org/10.1007/s11665-019-04242-5

1059-9495/$19.00

Multiaxial High Cycle Fatigue Criteria Based on Fracture Plane Identification: Applicability to Metallic Materials

Marcos V. Pereira, Fathi A. Darwish, Maria C. Teixeira, and Roberta A. Gonçalves

(Submitted February 18, 2019; in revised form July 11, 2019)

Two multiaxial high cycle fatigue criteria pertaining to the critical plane-based approach are reviewed. The models were proposed by Carpinteri and Spagnoli (C&S) and Liu and Mahadevan (L&M), and unlike other models based on the same approach, they have the critical plane directly correlated with the fatigue fracture plane. As the aim of this study is mainly to compare their capability to predict fatigue failure, the two models were applied to a number of published experimental fatigue tests, involving synchronous sinusoidal in-phase and out-of-phase bending and torsion. The results indicate that both models possess good predictive capability under fully reversed stresses, with the L&M model being on the average slightly more conservative. Applying, to the same loading conditions, a mesoscopic scale-based approach proposed by Papadopoulos, one can verify that its predictive capability is as good as those corresponding to the C&S and L&M criteria. However, in the presence of superimposed mean stresses, the capability of these two models to predict fatigue behavior is seen to be considerably lower than that detected for Papadopoulos'.

Keywords C&S criterion, critical plane, error index, fatigue limit state, fracture plane, L&M criterion, principal stresses

1. Introduction

Historically, the evaluation of the fatigue behavior of metallic materials was based on the determination of uniaxial fatigue test parameters for life prediction. However, many mechanical components, such as railroad wheels, crankshafts, axles and turbine blades, are expected to experience time-varying multiaxial stresses during their in-service lifetime. Accordingly, the need has been arising, over many decades, to introduce multiaxial fatigue damage criteria capable of predicting fatigue failure under such loading conditions. These criteria can be divided into three groups: stress-based, strain-based and energy-based models (Ref 1). Since the main focus in the present work is multiaxial high cycle fatigue, where most mechanical components are expected to operate under elastic stress levels, only stress-based models are considered.

Generalization of the fatigue limit concept, so as to englobe multiaxial loading conditions within the domain of stress-based models, is seen to be compatible with the notion of dividing the whole stress space in two parts, namely safe and unsafe. The safe part, containing the origin, is to be bounded by a closed surface, and the fatigue criterion can thus be expressed in terms of an inequality whose satisfaction signifies that the stress state induced by the external cyclic loading remains within the safe part of the stress space.

The stress-based approach, which is popularly used in high cycle fatigue analysis, englobes a large number of models that can be divided into four groups based on empirical equivalent stress, stress invariants, average stress and critical plane stress (Ref 1). Several reviews of multiaxial fatigue damage criteria, including stress-based models, can be found in the literature (Ref 2-6). In the present study, two stress-based high cycle fatigue models, namely Liu and Mahadevan (L&M) (Ref 1) and Carpinteri and Spagnoli (C&S) (Ref 6-9), both belonging to the critical plane approach, are reviewed with the underlying purpose of comparing their applicability to predicting high cycle fatigue behavior of metallic materials. Both models are, in fact, applicable to a wide spectrum of materials ranging from very ductile to extremely hard metallic alloys (Ref 1, 6). Accordingly, the comparison can be made by applying the two models to a number of experimental constant amplitude cyclic loading conditions available in the literature (Ref 10-12). These involve synchronous sinusoidal in-phase and out-of-phase bending and torsion applied to a variety of metallic materials with different fatigue behaviors. At this point, it needs to be mentioned that all of the selected loading conditions correspond to the fatigue limit state above which fatigue failure occurs and below which fatigue life extends over a very high number of cycles, in analogy with the fatigue limit state for uniaxial loading of smooth (unnotched) specimens. However, one may also point out that the C&S criterion, which has been used for fatigue assessment of both smooth and notched structural components, has also been extended to assess the fatigue behavior of welded joints under in-phase and out-of-phase loadings and more recently to evaluate fatigue life under multiaxial random loading conditions (Ref 9, 13-15).

Critical plane-based models depend for their application on the prior identification of the critical plane, where fatigue damage can occur leading to crack nucleation. One can therefore proceed to calculate the normal and shear stress amplitudes as well as the mean stresses acting on the critical plane, and fatigue failure assessment can thus be presented in

Marcos V. Pereira, Maria C. Teixeira, and **Roberta A. Gonçalves**, Department of Chemical and Materials Engineering, Catholic University of Rio de Janeiro, Rua Marques de São Vicente, 225, Rio de Janeiro, RJ 22453-901, Brazil; and **Fathi A. Darwish**, Department of Civil Engineering, Fluminense Federal University, Rua Passo da Patria, 156, Niterói, RJ 24210-240, Brazil. Contact e-mails: marcospe@gmail.com and mclaract@gmail.com.

Published online: 31 July 2019

the form of inequality. The relative difference between the two sides of the inequality is referred to as the error index, and, for a given fatigue limit state, it may be nil, positive or negative. As the two models in question are to be applied simultaneously to a given loading condition, a comparison of the error index involved is expected to provide a good assessment of their predictive capabilities in defining the fatigue behavior.

Finally, the critical plane orientation determined for each of the two models is presented in comparison with that of the fracture plane, for the loading conditions involved.

2. Review of the C&S and L&M Multiaxial Fatigue Criteria

The inequalities representative of the C&S and L&M models are given, respectively, by expressions (1) and (2) (Ref 1, 6):

$$\sqrt{N_{\max}^2 + \left(\frac{f_{-1}}{t_{-1}}\right)^2 C_a^2} \leq f_{-1} \qquad \text{(Eq 1)}$$

$$\sqrt{\left[\frac{N_a\left(1+\eta\frac{N_m}{f_{-1}}\right)}{f_{-1}}\right]^2 + \left(\frac{C_a}{t_{-1}}\right)^2 + k\left(\frac{H_a}{f_{-1}}\right)^2} \leq \lambda \qquad \text{(Eq 2)}$$

where C_a, N_a and H_a are, respectively, the shear stress, normal stress and hydrostatic stress amplitudes acting on the critical plane. Accordingly, the application of any of these two models depends on the prior identification of the corresponding critical plane. N_m is the mean normal stress acting on the same plane, and hence, $N_{\max}$ is given by

$$N_{\max} = N_a + N_m \qquad \text{(Eq 3)}$$

The constants η and λ in expression (2) are material parameters which depend exclusively on the fatigue limits for fully reversed bending f_{-1} and fully reversed torsion t_{-1}, as indicated by Eq 4 and 5 (Ref 1).

$$\eta = \frac{3}{4} + \frac{1}{4}\left[\frac{\left(\sqrt{3} - \frac{f_{-1}}{t_{-1}}\right)}{\sqrt{3}-1}\right] \qquad \text{(Eq 4)}$$

$$\lambda = \left[\cos^2(2\delta)s^2 + \sin^2(2\delta)\right]^{1/2} \qquad \text{(Eq 5)}$$

The constant δ in Eq 5 refers to the angle between the fracture and critical planes and, as shown later, is a function of s, which is the ratio t_{-1}/f_{-1}. Finally, it should be mentioned that Eq 4 is valid for $s \leq 1$ and that for $s \geq 1$, η is taken to be unity (Ref 1). For most metallic materials, where $t_{-1} \leq f_{-1}$, the constant k, as defined by the L&M model, is equivalent to zero and, on the other hand for $f_{-1} < t_{-1}$, k is given by the following (Ref 1).

$$k = 9(s^2 - 1)$$

More recently, with the evolution of the C&S criterion (Ref 9), $N_{\max}$ in expression (1) can be replaced by the parameter $N_{a,\text{eq}}$, which accounts for the effect of the mean normal stress as given below

$$N_{a,\text{eq}} = N_a + f_{-1}\left(\frac{N_m}{\sigma_u}\right) \qquad \text{(Eq 6)}$$

where σ_u is the ultimate tensile strength of the material. Equation 6 takes into account the linear relationship (proposed by Goodman (Ref 16)) between normal stress amplitude and normal stress mean value (Ref 9).

2.1 Critical Plane Determination

Critical plane identification for both models depends on knowing the fracture plane as well as the angular relationship between the two planes. Determination of the fracture plane is therefore an essential first step toward identifying the critical plane.

Correlation between the fatigue fracture plane and the average principal stress directions has been analyzed by Carpinteri et al. (Ref 9) for hard metals under out-of-phase sinusoidal bending and torsion. While the fracture plane orientation was experimentally identified, the average principal stress directions were determined by employing appropriate weight functions (Ref 9), and the results obtained have led to the conclusion that the normal to the fracture plane agrees with the weighted mean direction of the maximum principal stress (Ref 9). By examining the difference between the calculated and experimentally measured angle that the normal to the fracture plane makes with the longitudinal axis of fatigue test specimens belonging to a variety of metallic materials, the results obtained were considered to be quite satisfactory (Ref 9). As indicated in this reference, the difference referred to above was found to vary from 1° to 13° for Swedish hard steel 982 FA specimens, from 0° to 37° for mild steel specimens and from 4° to 8° for gray cast iron specimens, and for low carbon steel, this variation was limited to zero.

In agreement with the definition proposed by McDiarmid (Ref 17), the fracture plane in the L&M model is identified as the plane on which the maximum principal stress achieves its greatest value. Considering the plane stress loading condition (Fig. 1), defined by the parameters σ_a, τ_a, σ_m, τ_m and β, where σ_a and τ_a are, respectively, the applied normal and shear stress amplitudes, σ_m and τ_m, are the corresponding mean stresses and β is the phase difference between the bend and torsion loading; the normal stress amplitude N_a and the normal stress mean value N_m acting on an arbitrary material plane oriented at an angle φ with respect to the vertical axis are given by (Ref 6)

$$N_m = \sigma_m \sin^2(\varphi) + \tau_m \sin(2\varphi) \qquad \text{(Eq 7)}$$

$$N_a = \sqrt{a^2 + b^2} \qquad \text{(Eq 8)}$$

with

$$a = \sigma_a \sin^2(\varphi) + \tau_a \cos(\beta)\sin(2\varphi) \qquad \text{(Eq 9)}$$

$$b = -\tau_a \sin(\beta)\sin(2\varphi) \qquad \text{(Eq 10)}$$

The fatigue fracture plane can thus be determined by maximizing $N_{\max}$, with respect to the angle φ, which can be achieved by enumeration by changing φ according to a given increment (0.1°). The orientation of the fracture plane can then be expressed in terms of the angle ψ_f between the normal to the fracture plane and the vertical axis. That is

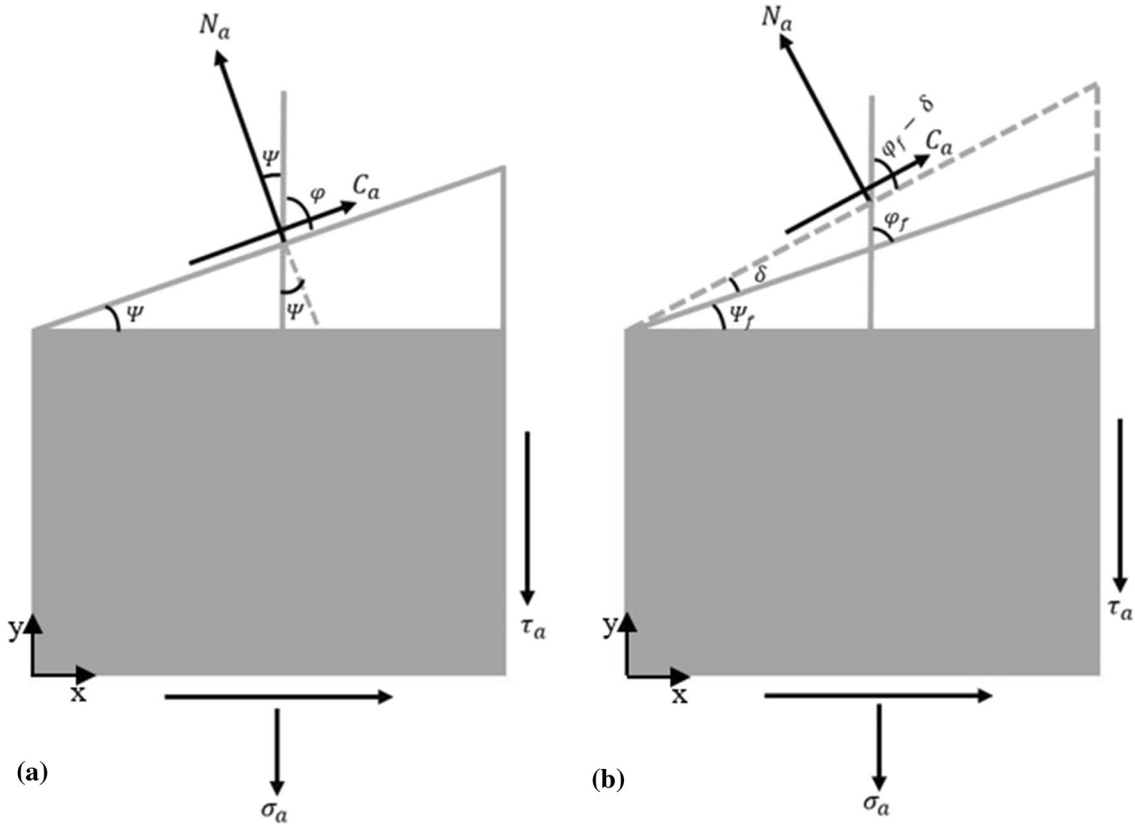

Fig. 1 Stresses acting on (a) a general material plane and (b) the critical plane

$$\Psi_f = \frac{\pi}{2} - \varphi_f, \qquad \text{(Eq 11)}$$

where φ_f is the angle associated with the greatest value of $N_{\max}$.

By adopting the above-mentioned procedure, it is hereby verified that the fracture plane as determined by maximizing $N_{\max}$ coincides with the plane perpendicular to the weighted mean direction of the maximum principal stress for the loading conditions reported in Ref (9). In fact, this was found to be true for all the loading conditions applied to Swedish hard steel, mild steel and gray cast iron specimens, as indicated in this reference. One can thus conclude that, for a given loading condition, both the C&S and L&M models predict the same fracture plane orientation, which can simply be identified by maximizing $N_{\max}$ with respect to the angle φ.

Once the fracture plane is determined, the critical plane will likewise be identified since the angle δ between the two planes is considered to be a material parameter. For the C&S model, δ is expressed as (Ref 6, 9)

$$\delta = \left[1 - \left(\frac{t_{-1}}{f_{-1}}\right)^2\right]\frac{3\pi}{8}, \qquad \text{(Eq 12)}$$

meaning that δ is nil for $t_{-1} = f_{-1}$, which is the case of extremely hard metals. For $t_{-1}/f_{-1} = 1/\sqrt{3}$, δ is equal to $\pi/4$, which is the border between hard and mild metals. As to the L&M model, the angle δ is given by (Ref 1)

$$\delta = \frac{1}{2}\cos^{-1}\left[\frac{-2 + \sqrt{4 - 4\left(\frac{1}{s^2} - 3\right)\left(5 - \frac{1}{s^2} - 4s^2\right)}}{2\left(5 - \frac{1}{s^2} - 4s^2\right)}\right] \qquad \text{(Eq 13)}$$

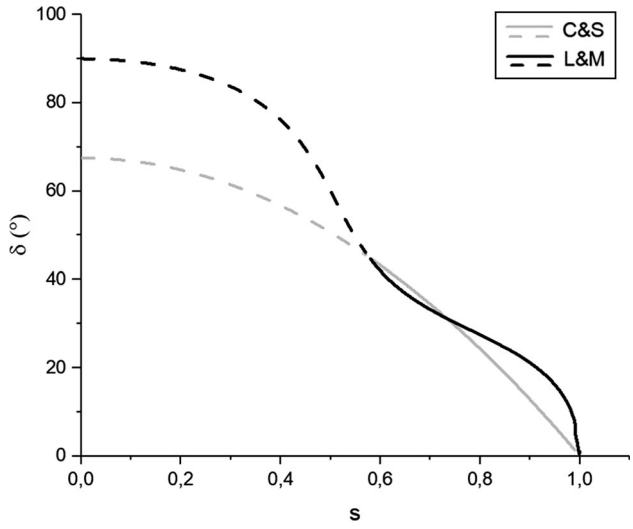

Fig. 2 Variation of the angle δ with the ratio t_{-1}/f_{-1}

Here δ is also nil for $s = 1$ and equivalent to $\pi/2$ for s tending to zero (Ref 1).

The variation of δ with s is depicted in Fig. 2, where one can observe the agreement between the two models for three s values within the range $1/\sqrt{3} \leq s \leq 1$, which corresponds to $45° \geq \delta \geq 0$. For $s < 1/\sqrt{3}$, the two models diverge from one another and accordingly the comparison between their applicabilities is limited, in the present study, to metallic materials with the ratio t_{-1}/f_{-1} pertaining to the range from $1/\sqrt{3}$ to 1.

Table 1 Loading conditions applied to hard steel_1

f_{-1}=313.9 MPa		t_{-1}=196.2 MPa		σ_u= 708.1 MPa	
Loading conditions	σ_a, MPa	σ_m, MPa	τ_a, MPa	τ_m, MPa	β, °
1	327.7	0	0	0	0
2	308	0	63.9	0	0
3	255.1	0	127.5	0	0
4	141.9	0	171.3	0	0
5	0	0	201.1	0	0
6	255.1	0	127.5	0	30
7	142	0	171.2	0	30
8	255.1	0	127.5	0	60
9	147.2	0	177.6	0	60
10	308	0	63.9	0	90
11	264.9	0	132.4	0	90
12	152.5	0	184.2	0	90

Table 2 Loading conditions applied to hard steel_2

f_{-1}=313.9 MPa		t_{-1}=196.2 MPa		σ_u= 608 MPa	
Loading conditions	σ_a, MPa	σ_m, MPa	τ_a, MPa	τ_m, MPa	β, °
1	138.1	0	167.1	0	0
2	140.4	0	169.9	0	30
3	145.7	0	176.3	0	60
4	150.2	0	181.7	0	90
5	245.3	0	122.6	0	0
6	249.7	0	124.8	0	30
7	252.4	0	126.2	0	60
8	258	0	129	0	90
9	299.1	0	62.8	0	0
10	304.5	0	63.9	0	90

Table 3 Loading conditions applied to mild steel

f_{-1}=235.4 MPa		t_{-1}=137.3 MPa		σ_u= 518.8 MPa	
Loading conditions	σ_a, MPa	σ_m, MPa	τ_a, MPa	τ_m, MPa	β, °
1	245.3	0	0	0	0
2	235.6	0	48.9	0	0
3	187.3	0	93.6	0	0
4	101.3	0	122.3	0	0
5	0	0	142.3	0	0
6	194.2	0	97.1	0	60
7	108.9	0	131.5	0	60
8	235.6	0	48.9	0	90
9	208.1	0	104.1	0	90
10	112.6	0	136	0	90

Knowing the angle δ, the critical plane orientation Ψ_c can be expressed, as shown in Fig. 1, by

$$\Psi_c = \Psi_f + \delta \quad \text{(Eq 14)}$$

or equivalently as

$$\varphi_c = \varphi_f - \delta \quad \text{(Eq 15)}$$

where δ is to be calculated using Eq 12 and 13 for the C&S and L&M criteria, respectively.

With the critical plane already identified, the stresses N_a and N_m acting normal to it can be determined by replacing φ in Eq 7, 9 and 10 by $\varphi_f - \delta$. In order to calculate the amplitude of the shear stress acting on the critical plane, one has, first, to consider a general material plane Δ (Fig. 1). During a cycle of synchronous out-of-phase sinusoidal biaxial normal and shear stress loading, the tip of the shear stress vector $\vec{C}$ describes, on Δ, a closed curve, which, as demonstrated in (Ref 3, 6),

Table 4 Loading conditions applied to gray cast iron

f_{-1}=96.1 MPa		t_{-1}=91.2 MPa		σ_u= 230 MPa	
Loading conditions	σ_a, MPa	σ_m, MPa	τ_a, MPa	τ_m, MPa	β, °
1	93.2	0	0	0	0
2	95.2	0	19.7	0	0
3	83.4	0	41.6	0	0
4	56.3	0	68.0	0	0
5	0	0	94.2	0	0
6	104.2	0	21.6	0	90
7	97.1	0	48.6	0	90
8	71.3	0	86.1	0	90

Table 5 Loading conditions applied to 42CrMo4

f_{-1}=398 MPa		t_{-1}=260 MPa		σ_u= 1025 MPa	
Loading conditions	σ_a, MPa	σ_m, MPa	τ_a, MPa	τ_m, MPa	β, °
1	328	0	157	0	0
2	286	0	137	0	90
3	233	0	224	0	0
4	213	0	205	0	90
5	266	0	128	128	0
6	283	0	136	136	90
7	333	0	160	160	180
8	280	280	134	0	0
9	271	271	130	0	90

Table 6 Loading conditions applied to 34Cr4

f_{-1}=410 MPa		t_{-1}=256 MPa		σ_u= 795 MPa	
Loading conditions	σ_a, MPa	σ_m, MPa	τ_a, MPa	τ_m, MPa	β, °
1	314	0	157	0	0
2	315	0	158	0	60
3	316	0	158	0	90
4	315	0	158	0	120
5	224	0	224	0	90
6	380	0	95	0	90
7	316	0	158	158	0
8	314	0	157	157	60
9	315	0	158	158	90
10	279	279	140	0	0
11	284	284	142	0	90
12	355	0	89	178	0
13	212	212	212	0	90
14	129	0	258	0	90

corresponds to an elliptic path. The semi-axes of the ellipse can be computed as (Ref 6).

$$C_{a,b} = \sqrt{\frac{f^2+g^2+p^2+q^2}{2} \pm \sqrt{\left(\frac{f^2+g^2+p^2+q^2}{2}\right)^2 - (fq-gp)^2}}$$

with the major semi-axis representing the shear stress amplitude C_a. The functions f, g, p and q are given by (Ref 6)

$$f = \frac{1}{2}\sin 2\theta\left[\sigma_{t,a}\cos\alpha\cos^2\varphi + \sigma_{l,a}\sin^2\varphi + \tau_a\cos\beta\sin 2\varphi\right]$$

$$g = -\frac{1}{2}\sin 2\theta\left[\sigma_{t,a}\sin\alpha\cos^2\varphi + \tau_a\sin\beta\sin 2\varphi\right]$$

$$p = \sin\theta\left[\frac{1}{2}\left(\sigma_{l,a} - \sigma_{t,a}\cos\alpha\right)\sin 2\varphi + \tau_a\cos\beta\cos 2\varphi\right]$$

$$q = -\sin\theta\left[-\frac{1}{2}\sigma_{t,a}\sin\alpha\sin 2\varphi + \tau_a\sin\beta\cos 2\varphi\right]$$

Table 7 Loading conditions applied to 30NCD16

f_{-1}=660 MPa		t_{-1}=410 MPa		σ_u= 1880 MPa	
Loading conditions	σ_a, MPa	σ_m, MPa	τ_a, MPa	τ_m, MPa	β, °
1	485	0	280	0	0
2	480	0	277	0	90
3	480	300	277	0	0
4	480	300	277	0	45
5	470	300	270	0	60
6	473	300	273	0	90
7	590	300	148	0	0
8	565	300	141	0	45
9	540	300	135	0	90
10	211	300	365	0	0

where θ is the angle between the normal to the plane Δ and the z-axis (normal to the x–y plane), $\sigma_{t,a}$ and $\sigma_{l,a}$ are, respectively, normal stress amplitudes along the x and y axes, i.e., transverse and longitudinal directions, and α is the phase difference between the normal stress components.

For the plane stress loading conditions in question, θ is equivalent to $\pi/2$, $\sigma_{t,a}$ is nil and $\sigma_{l,a}$ is replaced by σ_a and hence f and g turn out to be nil and p and q reduce to

$$p = \frac{1}{2}\sigma_a \sin(2\varphi) + \tau_a \cos(\beta)\cos(2\varphi) \quad \text{(Eq 16)}$$

$$q = -\tau_a \sin(\beta)\cos(2\varphi) \quad \text{(Eq 17)}$$

with C_a expressed as

$$C_a = \sqrt{p^2 + q^2} \quad \text{(Eq 18)}$$

and the amplitude of the shear stress acting on the critical plane is obtained for the p and q values calculated by replacing φ in expressions (16) and (17) by $\varphi_c = \varphi_f - \delta$.

The C&S and L&M criteria can thus be applied by substituting N_a, N_m and C_a values, calculated for each model, in the inequalities given, respectively, by expressions (1) and (2). It is to be noted that the term involving H_a in expression (2) vanishes in virtue of the fact that the constant k is nil for metallic materials. The error index I, which refers to the relative difference between the two sides of the inequalities, can be estimated as

$$I = \frac{\text{left hand side} - \text{right hand side}}{\text{right hand side}} \times 100 \quad \text{(Eq 19)}$$

Aiming at comparing the predictive capability of the models in question with other pertinent models, a mesoscopic scale-based criterion developed by Papadopoulos et al. (Ref 3) and Papadopoulos (Ref 18, 19) is to be applied to the same experimental loading conditions. The inequality representative of Papadopoulos' criterion is expressed directly in terms of the applied stress amplitudes and mean normal stress as given below:

$$\sqrt{\frac{\sigma_a^2}{3} + \tau_a^2} + \alpha\frac{\sigma_a + \sigma_m}{3} \leq t_{-1} \quad \text{(Eq 20)}$$

where

$$\alpha = \left(\frac{3t_{-1}}{f_{-1}}\right) - \sqrt{3} \quad \text{(Eq 21)}$$

The application of Papadopoulos' criterion can be made by substituting σ_a, τ_a and σ_m in expression (20) and the corresponding error index I estimated from Eq 19. It should be noted though that the validity of the above criterion is limited to metals for which the inequality $1/\sqrt{3} \leq t_{-1}/f_{-1} \leq 0.8$ holds and, therefore, cannot be applied to a material like gray cast iron, where the ratio t_{-1}/f_{-1} is close to unity.

It is important to point out that the error index-based comparison, which is here proposed to be carried out between the models in question, can be made in terms of conventional fatigue limit state under multiaxial loading, where the fatigue life extends over a high number of cycles ($> 10^6$). With the error index I tending to zero, a given criterion is considered to be in good agreement with the experiment carried out for a set of cyclic bend and torsion loading. Positive I values, on the one hand, are indicative of fatigue failure in a situation where failure is not observed, and hence, the criterion is considered to be conservative. Negative I values, on the other hand, indicate that an adopted criterion is nonconservative, as it may permit an increase in the applied cyclic loads thus leading to higher risk of fatigue failure.

3. Applying the Models

The loading conditions, which are listed in Tables 1, 2, 3, 4, 5, 6, and 7, correspond to the fatigue resistance limits of seven different metallic materials, and hence, they can be used to test the applicability of the criteria in question. As mentioned earlier, these loading conditions come from various sources (Ref 10-12) and involve both in-phase and out-of-phase synchronous sinusoidal bending and torsion, whereby normal and shear stress components belonging to the same plane act cyclically on the fatigue specimens. For smooth unnotched fatigue specimens, 3D stresses are not likely to arise and the normal to the critical plane continues to belong to the x–y plane (Fig. 1). As presented in Tables 1, 2, 3, 4, 5, 6 and 7, the loading parameters include both stress amplitudes and mean stress values together with the phase difference between the normal and shear stress components. Ultimate tensile strength and fatigue resistance limits (f_{-1} and t_{-1}) are also listed in these tables.

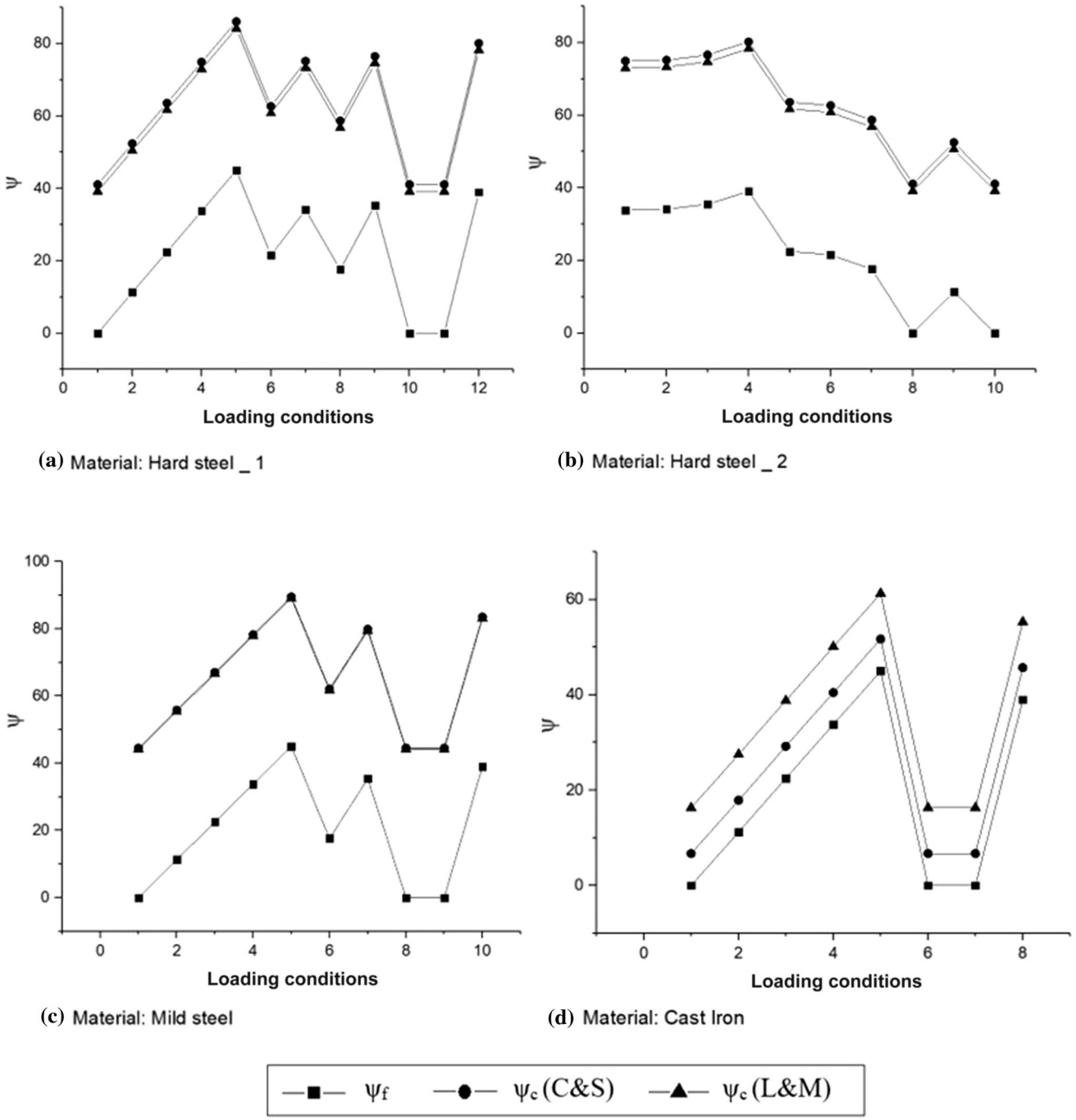

Fig. 3 Fracture and critical plane orientations, as defined, respectively, by ψ_f and ψ_c, for the different loading conditions: (a) hard steel_1; (b) hard steel_2; (c) mild steel and (d) cast iron

The fracture plane orientation, corresponding to the loading conditions in question, is presented in Fig. 3 and 4, in terms of ψ_f which is the complementary angle to φ_f. The critical plane orientation, on the other hand, is presented in the same figure in terms of the angle ψ_c which is obtained by adding δ to ψ_f.

The values of the error index I corresponding to the different loading conditions are presented in Fig. 5 and 6 for the variety of materials involved. In addition to the error index evaluated for the C&S, L&M and Papadopoulos models, this figure also depicts the I values obtained by replacing $N_{\max}$ by $N_{a,\mathrm{eq}}$ (Eq 6), in virtue of the evolution of the C&S criterion.

3.1 Discussing the Error Index

Although it can be stated that, except for a few cases, the majority of the I values shown in Fig. 5 and 6 are situated within the range ± 10%, indicating fair predictive capabilities of the criteria in question, one should point out that no common pattern is observed for the variation of the error index, for the materials involved. This is also reflected in the average I value, which for a given model varies considerably from one material to another.

As the loading conditions applied to hard steels (Tables 1 and 2) correspond to fully reversed bending and torsion, the

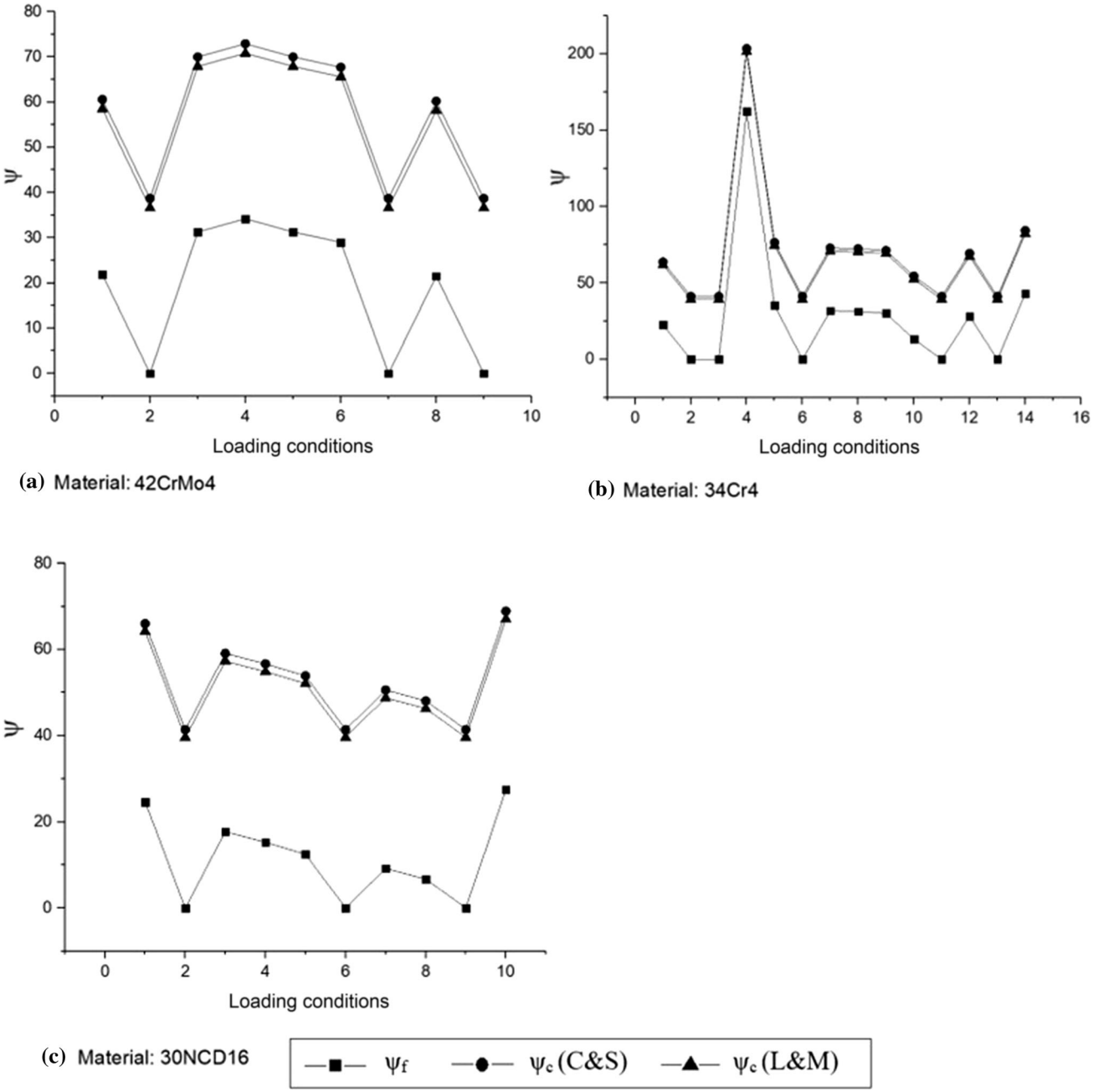

Fig. 4 Fracture and critical plane orientations, as defined, respectively, by ψ_f and ψ_c, for the different loading conditions: (a) 42CrMo4; (b) 34Cr4 and (c) 30NCD16

modified and original C&S criteria turn out to be equivalent. Besides being close to each other, the individual error index values associated with both C&S and L&M criteria are all situated in the range $-10 < I < 5$, which indicates fairly good capability for predicting fatigue behavior of hard steels. However, based on the observation that the average error index for these two models is negative, they may be considered as being less safe compared to the Papadopoulos criterion seen to be moderately conservative.

In the case of mild steel, for which the ratio t_{-1}/f_{-1} amounts to 0.584, the angle δ is given by 44.79° and 44.61° for C&S and L&M, respectively. For fully reversed loading, this results in having the same error index for both criteria (Fig. 3 and 4). On the average, these two models may be considered to be slightly conservative, but much less so if compared to Papadopoulos' (Fig. 5 and 6). Specifically, for out-of-phase loading, the error index I is confined to $-3 < I < 2$ for C&S and L&M, but turns out to be more conservative on applying the Papadopoulos criterion.

The application of the models to gray cast iron subjected to fully reversed loading indicates that the L&M is more conservative than C&S. This is manifested by comparing the individual I values (Fig. 5 and 6) as well as their overall averages (Fig. 7).

With regard to the 42CrMo4 and 34Cr4 alloys, one can observe that, for more than half of the loading conditions involved, the error indices associated with applying the C&S and L&M criteria are highly negative, i.e., $I < -10\%$.

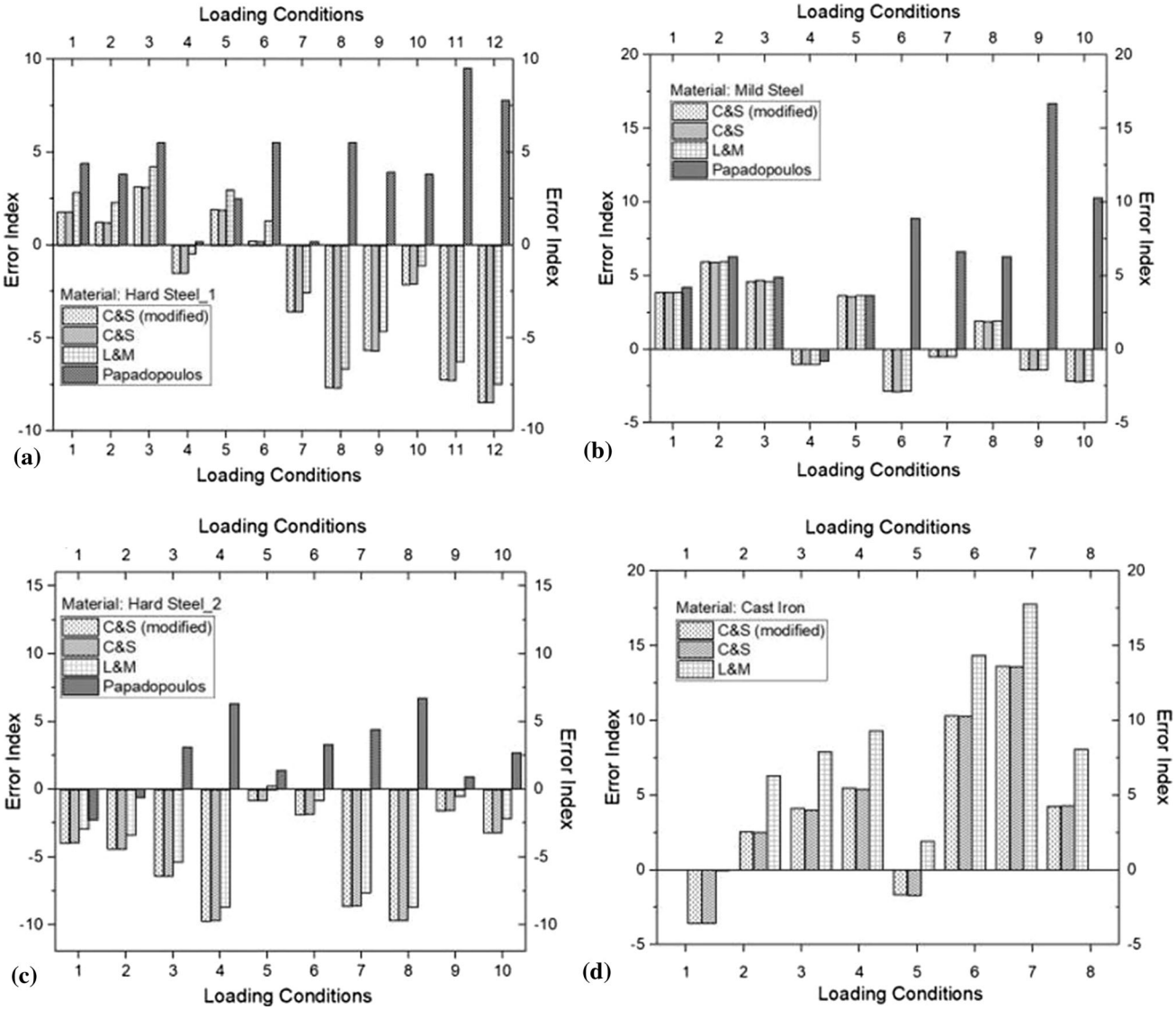

Fig. 5 Error index associated with applying the models, in question, to the individual loading conditions: (a) hard steel_1; (b) mild steel; (c) hard steel_2 and (d) cast iron

Further, one may also observe that, for fully reversed loading, the two models result in close values of I. However, for loading conditions involving mean stresses, the index predicted by the original C&S is appreciably different from that obtained by applying the L&M. The use of the modified C&S criterion in this case results in approximating the two indices to one another. Compared to Papadopoulos', both C&S and L&M criteria are seen to possess far less predictive capability for the two alloys, which is also confirmed by the average I values reported in Fig. 7.

Finally, regarding the 30NCD16 alloy, one can notice that, except for a single out-of-phase loading condition, the error index is limited to $-10 < I < 9$ for both C&S and L&M criteria. For loading conditions involving a mean stress σ_m acting during cyclic loading, the modified C&S criterion implies in error index closer to that predicted by L&M. It should be noted, though, that this may occasionally signify, as can be verified from Fig. 5–7, a lower predictive capability of the modified C&S criterion in comparison with the original one.

4. Conclusions

Based on the comparative study carried out in the present work, the following conclusions can be drawn:

Fracture plane orientation, which is exclusively dependent on the fatigue loading parameters, can be identified in both C&S and L&M models as the plane on which the maximum principal stress achieves its greatest value during cyclic loading.

The predictive capability of the models, in case of fully reversed bend and torsion loading, depends primarily on the magnitude of the angle between the fracture and critical planes, which is inherent to each model. Although the error index values for this type of loading are shown to be very close, the L&M model is considered to be slightly more conservative than its C&S counterpart. However, both models are considered to be much less so, compared Papadopoulos'.

For loading conditions involving the presence of mean stresses, the original C&S criterion is seen to possess better

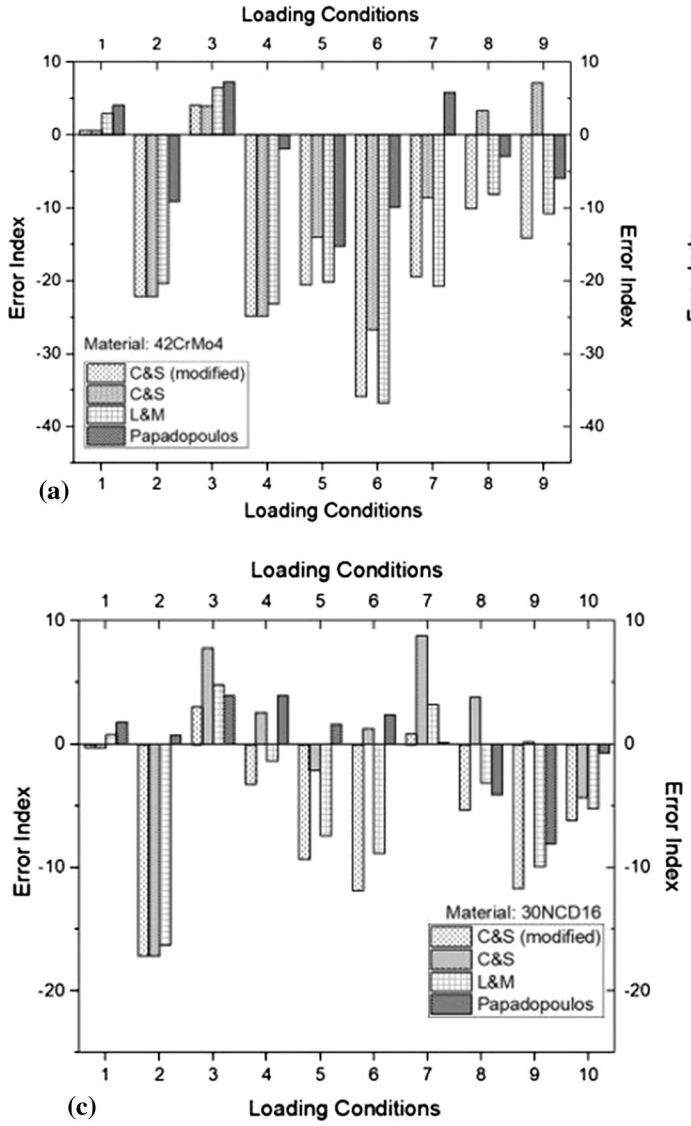

Fig. 6 Error index associated with applying the models, in question, to the individual loading conditions: (a) 42CrMo4; (b) 34Cr4 and (c) 30NCD16

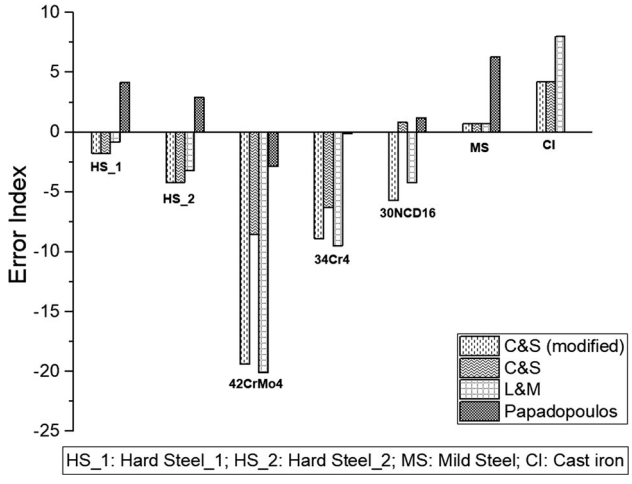

Fig. 7 Average error index associated with the models for each of the materials involved

predictive capability than its L&M counterpart. However, on adopting the modified C&S version, the error index gets closer to that predicted by the L&M model, which may occasionally signify lower predictive capability of the modified C&S version relative to the original one. Finally, one can conclude that, in addition to being more conservative, the Papadopoulos model possesses a better capability for predicting fatigue behavior for this type of loading in comparison with both C&S and L&M criteria.

Acknowledgments

This work was developed within the scope of the Research and Technological Development of the Brazilian Electric Energy Sector Program regulated by ANEEL, with the support of the Eneva Companies—Pecém II Energy Generation S.A., Itaqui Energy Generation S.A. and Parnaíba I, II and III Energy Generation S.A.

References

1. Y. Liu and S. Mahadevan, Multiaxial High-Cycle Fatigue Criterion and Life Prediction for Metals, *Int. J. Fatigue*, 2005, **27**, p 790–800
2. Y.S. Garud, Multiaxial Fatigue: A Survey of the State-of-the-Art, *J. Test. Eval.*, 1981, **9**, p 165–178
3. I.V. Papadopoulos, P. Davoli, C. Gorla, M. Filippini, and A. Bernasconi, A Comparative Study of Multiaxial High Cycle Fatigue Criteria for Metals, *Int. J. Fatigue*, 1997, **19**, p 219–235
4. Y.Y. Wang and W.X. Yao, Evaluation and Comparison of Several Multiaxial Fatigue Criteria, *Int. J. Fatigue*, 2004, **26**, p 17–25
5. B.R. You and S.B. Lee, A Critical Review on Multiaxial Fatigue Assessments of Metals, *Int. J. Fatigue*, 1996, **18**, p 235–244
6. A. Carpinteri and A. Spagnoli, Multiaxial High Cycle Fatigue Criterion for Hard Metals, *Int. J. Fatigue*, 2001, **23**, p 135–145
7. A. Carpinteri, R. Brighenti, and A. Spagnoli, A Fracture Plane Approach in Multiaxial High Cycle Fatigue of Metals, *Fatigue Fract. Eng. Mater. Struct.*, 2000, **23**, p 355–364
8. A. Carpinteri, A. Spagnoli, and S. Vantadori, Multiaxial Fatigue Assessment Using a Simplified Critical Plane-Based Criterion, *Int. J. Fatigue*, 2011, **33**, p 969–976
9. A. Carpinteri, A. Spagnoli, S. Vantadori, and C. Bagni, Structural Integrity Assessment of Metallic Components Under Multiaxial Fatigue: The C-S Cri-terion and its Evolution, *Fatigue Fract. Eng. Mater. Struct.*, 2013, **36**, p 870–883
10. T. Nishihara and M. Kawamoto, The Strength of Metals Under Combined Alternating Bending and Torsion with Phase Difference, *Mem College Eng Kyoto Imp Univ*, 1945, **11**, p 85–112 (Cited in Ref [3,6])
11. H. Zenner, R. Heidenreich, and I.Z. Richter, Dauerschwingfestigkeit bei nichtsynchroner mehrachsinger beanspruchung, *Werkstofftech*, 1985, **16**, p 101 (Cited in Ref [3])
12. C. Froustey and S. Lasserre, Multiaxial Fatigue Endurance of 30NCD16 Steel, *Int. J. Fatigue*, 1989, **11**, p 169–175
13. A. Carpinteri, A. Spagnoli, S. Vantadori, and D. Viappiani, A Multiaxial Criterion for Notch High-Cycle Fatigue Using a Critical-Point Method, *Eng. Fract. Mech.*, 2008, **75**, p 191–199
14. A. Carpinteri, A. Spagnoli, and S. Vantadori, Multiaxial Criteria Fatigue Life Estimation in Welded Joints Using the Critical Plane Approach, *Int. J. Fatigue*, 2009, **31**, p 188–196
15. A. Carpinteri, G. Fortese, C. Roncher, D. Scorza, A. Spagnoli, and S. Vantadori, Fatigue Life Evaluation of Metallic Structures Under Multiaxial Random Loading, *Int. J. Fatigue*, 2016, **90**, p 191–199
16. J. Schijve, *Fatigue of Structural Materials*, Springer, Berlin, 2009
17. D.L. McDiarmid, Fatigue Under Out-of-Phase Bending and Torsion, *Fa-tigue Fract Eng Mater Struct*, 1987, **9**, p 457–475
18. I.V. Papadopoulos, Critical Plane Approach in High Cycle Fatigue: On the Definition of the Amplitude and Mean Value of the Shear Stress Acting on the Critical Plane, *Fatigue Fract. Eng. Mater. Struct.*, 1998, **21**, p 269–285
19. I.V. Papadopoulos, Long Life Fatigue under Multiaxial Loading, *Int J Fa-tigue*, 2001, **23**, p 839–849